Research Square

Preprints are preliminary reports that have not undergone peer review.
They should not be considered conclusive, used to inform clinical practice,
or referenced by the media as validated information.

Urban Heat and Vegetation Dynamics in Rajshahi City: A Google Earth Engine- Based Analysis from 2005 to 2024

Roni Roy

roniroy.geo@gmail.com

University of Rajshahi

Research Article

Keywords: LST, UHI, UTFVI, Google Earth Engine, Rajshahi City Corporation

Posted Date: March 3rd, 2026

DOI: https://doi.org/10.21203/rs.3.rs-8949028/v1

License: This work is licensed under a Creative Commons Attribution 4.0 International License.
Read Full License

Additional Declarations: No competing interests reported.

Urban Heat and Vegetation Dynamics in Rajshahi City: A Google Earth Engine-Based Analysis from 2005 to 2024

Roni Roy[1]*

[1]Department of Geology and Mining, University of Rajshahi, Rajshahi-6205, Bangladesh.

*Corresponding author email address: roniroy.geo@gmail.com

Abstract

Understanding the spatiotemporal dynamics of urban surface temperature and vegetation health is vital for sustainable urban planning, particularly in rapidly developing cities such as Rajshahi. This study analyzes long-term changes in Land Surface Temperature (LST), Normalized Difference Vegetation Index (NDVI), Health Vegetation Index (HVI), Urban Heat Island (UHI), and Urban Thermal Field Variance Index (UTFVI) within Rajshahi City Corporation over 20 years, from 2005 to 2024. Multitemporal Landsat imagery and the cloud-based Google Earth Engine (GEE) platform were employed to examine three key time points 2005, 2015, and 2024, and assess the impacts of urban expansion and vegetation loss on the urban thermal environment. Results reveal a consistent increase in both LST and UHI intensity. In 2005, LST ranged from 23.49°C to 38.57°C, rising to 24.21°C to 41.34°C by 2024. Correspondingly, UHI values intensified from a range of –1.063 to 2.458 in 2005 to –3.79 to 4.97 in 2024. NDVI and HVI values declined in the urban core, indicating vegetation degradation, while UTFVI patterns reflected increasing ecological thermal stress, especially in densely built-up areas. Spatial analyses confirmed that impervious surfaces are associated with higher heat stress, whereas vegetated zones help mitigate thermal impact. The integration of remote sensing indices with GEE's processing capabilities offers an efficient and scalable approach for monitoring urban climate dynamics. These findings provide actionable insights for urban planners and policymakers to implement nature-based solutions, improve thermal comfort, and enhance ecological resilience in Rajshahi's evolving urban landscape.

Key Word: LST, UHI, UTFVI, Google Earth Engine, Rajshahi City Corporation.

Introduction

The conversion of natural landscapes into impermeable built environments due to rapid urbanization has become a significant driver of land cover change, significantly altering surface thermal regimes and local microclimates (Grimmond, 2007; Oke, 1982). When concrete, asphalt, and other artificial materials are used in place of vegetated surfaces in urban areas, surface heat

retention rises, evapotranspiration falls, and natural energy balances are upset. This results in higher Land Surface Temperatures (LST) and the development of Urban Heat Islands (UHI) (Santamouris, 2015; Voogt & Oke, 2003). Due to its ability to shade surfaces, promote evapotranspiration, and change surface albedo, vegetation is an essential moderator of urban heat (Weng, 2009; Li et al., 2018). Vegetation cover, health, and stress can be measured with the help of remote sensing indices like the Normalized Difference Vegetation Index (NDVI), Vegetation Condition Index (VCI), Temperature Condition Index (TCI), and Vegetation Health Index (VHI) (Karnieli et al., 2009; Sobrino et al., 2020). Whereas VCI highlights stress or deterioration, NDVI shows photosynthetic activity and vegetation density. VHI combines VCI and TCI to provide a comprehensive assessment of vegetation health under anthropogenic and climatic stressors. TCI measures thermal stress by comparing LST with long-term temperature extremes (Kogan, 1995; Liu & Kogan, 2002). Researchers can identify vulnerable areas and comprehend how vegetation reduces urban heating by combining these indices with LST and thermal stress indicators such as the Urban Thermal Field Variance Index (UTFVI) (Bala et al., 2021).

Bangladesh has seen a surge in urbanization, especially in the past 20 years, as built-up areas in megacities and medium-sized cities have rapidly expanded. The majority of research has focused on Dhaka and Chattogram, but medium-sized cities like Rajshahi are experiencing significant land cover change, which has quantifiable effects on UHI (Rahman et al., 2022; Roy et al., 2024). According to (Marufuzzaman et al., 2021), Rajshahi's built-up area more than doubled between 1998 and 2018, and LST increased at the same time. According to (M. R. Rahman & Mark, 2025), densely populated areas devoid of greenery showed notable warming, whereas regions with high vegetation density maintained lower surface temperatures. To assess these dynamics, vegetation indices have been used extensively. VCI identifies stressed vegetation, TCI highlights heat-affected areas, VHI integrates both to evaluate overall vegetation health under urbanization pressure, and NDVI provides spatial-temporal patterns of greenness (Liu & Kogan, 2002). In Rajshahi, (M. M. Rahman & Hasan, 2024) showed that lower daytime LST was correlated with higher VHI values, suggesting that vegetation considerably reduces surface heating. (Sadat et al., 2024) demonstrated through ENVI-Met simulations that urban greening measures, such as green roofs and street trees, could lower near-surface air temperatures by as much as 10 K in specific areas. These studies demonstrate the significance of integrating various indices to evaluate

vegetation stress and thermal interactions, as well as the crucial role that vegetation plays in urban thermal regulation.

Multi-temporal, high-resolution data are necessary for long-term monitoring of vegetation, urban thermal stress, and LST. With Landsat satellites providing reliable imagery since the 1980s, remote sensing offers an efficient method that can be used to evaluate LST, NDVI, VCI, TCI, and VHI over long periods of time (Gorelick et al., 2017). Researchers can efficiently process large datasets, perform classification, index calculation, and spatiotemporal trend mapping via cloud-based platforms like Google Earth Engine (GEE), which enable scalable, reproducible analyses (Rizwan et al., 2008; Chakraborty & Lee, 2018). These methods have been used in a number of studies conducted in Bangladesh. M. R. Rahman & Mark, 2025 mapped Rajshahi's urban heat distribution and vegetation dynamics at high spatial resolution using Landsat-derived LST and NDVI. Other studies in Chattogram showed the potential of cloud-based geospatial analysis in data-scarce urban contexts by using GEE with machine learning algorithms to track LULC and thermal indices over a 20-year period (Yang et al., 2022). Notwithstanding these developments, there are still few thorough studies in Rajshahi that combine LST, NDVI, VCI, TCI, VHI, UHI, and UTFVI at the ward level. The distribution of urban heat stress is not uniform; socioeconomic factors, built-up density, and vegetation cover all effect intra-city variability (Imhoff et al., 2009; Zhou et al., 2014). Heat-vulnerable areas can be finely identified through ward-level assessments, allowing for focused mitigation measures. According to earlier studies, combining vegetation and thermal indices (NDVI, VCI, TCI, and VHI) with LST and UTFVI improves knowledge of local thermal stress and directs evidence-based urban planning (Bala et al., 2021). Since urban growth and vegetation loss have been spatially heterogeneous, resulting in hotspots of thermal stress, especially in central and northern wards, ward-level monitoring is crucial for Rajshahi (Rahman et al., 2022). The literature identifies a number of gaps that spur this investigation Ward-Level Analysis: In Bangladesh, the majority of research focuses on coarse zonal averages or city-wide averages, which limits our understanding of intra-city heterogeneity. Precise urban planning requires ward-by-ward, fine-scale assessment. Few studies examine LST, NDVI, VCI, TCI, VHI, UHI, and UTFVI together over extended periods of time. A more complex understanding of vegetation-mediated thermal regulation is possible by combining these indices. Recent Temporal Coverage: In order to capture the most recent urban growth and environmental changes, updated analysis up to 2024 is crucial, as many studies cover periods prior to 2020. Policy-Relevant

Mapping: Spatially explicit, ward-level evidence is necessary to convert scientific findings into workable urban greening and heat mitigation strategies.

2. Study area

Rajshahi City Corporation (RCC) is a self-administered local government body responsible for managing the affairs of Rajshahi City, one of the major divisional city corporations in Bangladesh (Fig. 1). The city is located between 24°20′ and 24°24′ N latitudes and 88°32′ and 88°40′ E longitudes, covering an area of approximately 96.72 km² on the northern bank of the Padma River (Banglapedia 2021; BBS 2013). The elevation of the area ranges from 15 to 19 m above mean sea level. Climatically, Rajshahi falls within the dry-wet tropical monsoonal zone, often termed

Figure 1. Study area map

the western dry zone of Bangladesh. It experiences a mean annual rainfall below 1524 mm, with temperatures ranging between 10 and 36°C. The highest temperatures usually occur during April and May (Clemett et al. 2006; Ferdous & Baten, 2012). RCC was officially established in 1991 and functions as the social, economic, and administrative hub of northern Bangladesh. The population increased from 388,811 in 2001 to 553,288 in 2022 (BBS 2022), reflecting rapid urbanization driven by employment opportunities, rural-to-urban migration, and small-scale industrial development (Al Rakib et al., 2020; Kafy et al., 2019). In recent decades, unplanned urban expansion has considerably transformed the city's land use and environmental conditions. Studies report a 19% decrease in green cover and an increase of nearly 9°C in maximum Land Surface Temperature (LST) over the past two decades, indicating a clear trend of urban heat intensification and environmental degradation (Kafy et al., 2020; RDA 2003, 2008; Dey et al., 2021).

3. Data and Processing

3.1 Data Sources

A cloud-based geospatial analytic tool, Google Earth Engine (GEE) can effectively handle massive amounts of temporal and spatial datasets (Sun et al., 2021; Rahaman & Venkatesh, 2020). Multi-temporal Landsat satellite imagery used in this investigation was obtained from the Google Earth Engine Data Catalogue (ee.ImageCollection). The Landsat 5 Thematic Mapper (TM), Landsat 7 Enhanced Thematic Mapper Plus (ETM+), and Landsat 8 Operational Land Imager/Thermal

Infrared Sensor (OLI/TIRS) datasets, respectively, represented the study years 2005, 2015, and 2024. For the analysis of vegetation conditions and land surface temperature (LST), these databases offer reliable long-term observations. Every image was chosen annually for each research year, from January to December, in order to reduce seasonal effects and guarantee temporal consistency.

3.2 Data Processing in Google Earth Engine

Google Earth Engine's JavaScript API was used to process each dataset. Image selection, preprocessing, index computation, and data export were all part of the processing pipeline. To effectively handle and analyze the data, a number of built-in GEE functions were used, including filterDate, filterBounds, map, reduce, clip, expression, print, and export. Quality assessment (QA) bands were used to exclude cloud-contaminated and shadow pixels. Using median compositing, which minimizes noise and lingering cloud effects, annual representative images were produced. All photos were resampled to a common spatial resolution and reprojected to a standard coordinate reference system to guarantee inter-annual comparability.

3.3 Derivation of Vegetation and Thermal Indices

Several spectral and thermal indices were developed from the Landsat data in order to assess vegetation dynamics and urban thermal features. To evaluate the density and health of the vegetation, the Normalized Difference Vegetation Index (NDVI) was computed. Using radiometric calibration, brightness temperature conversion, and NDVI-based land surface emissivity correction, Land Surface Temperature (LST) was calculated using thermal infrared bands. In order to assess vegetative stress levels, the vegetative Health Index (VHI) was calculated by combining NDVI and LST. By examining the spatial differences in LST between vegetative and built-up areas, the intensity of the Urban Heat Island (UHI) was determined. In order to categorize thermal comfort levels and ecological stress conditions in the urban environment, the Urban Thermal Field Variance Index (UTFVI) was also computed. All indices were generated on an annual basis for the years 2005, 2015, and 2024.

3. Methodology

This study analyzed vegetation dynamics and urban heat patterns in Rajshahi City for the years 2005, 2015, and 2024 using Google Earth Engine (GEE). The GEE will work in JavaScript and Python; likewise, in this study, all data have been processed in GEE through the JavaScript API

and exported to Google Drive as a TIFF file. Landsat imagery was used to compute NDVI, LST, VHI, UHI, and UTFVI on an annual basis (January–December) and spatial visualization in ArcGIS 10.8.

3.1 Image Collection and Preprocessing

Landsat 5 Thematic Mapper (TM) provided surface reflectance data for 2005; Landsat 8 OLI/TIRS provided data for 2015 and 2024. Every image was geographically cropped to the Rajshahi City Corporation limit and filtered by date (January–December for each individual year). With a spatial resolution of 30 meters, Landsat 8 offers multispectral imagery that is appropriate for environmental investigation at the urban scale. Band 4 (Red: 0.64–0.67 μm), Band 5 (Near Infrared: 0.85–0.88 μm), and Band 10 (Thermal Infrared: 10.6–11.19 μm) were used in this investigation. Band 5 records near-infrared reflectance strongly linked to healthy vegetation, Band 4 records visible red wavelengths sensitive to chlorophyll absorption, and Band 10 measures emitted thermal radiation used to determine land surface temperature instead of atmosphere air temperature.

Similarly, using Landsat 5 TM, NDVI and LST for 2005 were derived using Band 3 (Red: 0.63–0.69 μm), Band 4 (NIR: 0.76–0.90 μm), and Band 6 (Thermal Infrared: 10.4–12.5 μm). In order to reduce cloud cover and preserve constant radiometric conditions, all Landsat sceneries were chosen mainly during the dry season. The QA_PIXEL quality assurance band was used to eliminate cloud and cloud-shadow pixels. In order to provide robust temporal representation and lessen the impact of noise and outliers, final image composites were created by computing annual median values for each year. The computational mapping process flowchart are shown in fig. 2.

Figure 2. Flowchart of data processing.

3.1.1. NDVI analysis

According to (Yang et al., 2017), plants influence variations in surface temperature by absorbing or reflecting solar radiation. Given the complexity of the interaction between NDVI and LST, this is a crucial topic of study (Ghobadi et al., 2013). One important metric for characterizing the spectrum shift in an area's vegetation cover is the NDVI (Khaliq et al., 2018). NDVI makes it easier to identify vegetated regions and assess the condition of the vegetation. Its foundation is the computation of vegetation reflection values, which range from -1 to + 1 (Kavlak et al., 2021)

utilizing the near-infrared (NIR) and RED bands (Sun et al., 2021). According to (Cetin & Yastikli, 2022), the NDVI values are computed using equation (1) below.

$$\text{NDVI} = \frac{(NIR-RED)}{(NIR+RED)} \quad (1)$$

$$Pv = \left(\frac{NDVI - NDVI_{min}}{NDVI_{max} - NDVI_{min}}\right)^2 \quad (2)$$

Solving for NDVI in Eq. (1), and substituting into Eq. (2), yields the proportion of vegetation Pv.

NDVImin refers to the previous result of NDVI minimum value while NDVImax refers the NDVI maximum value. Afterwards, the next step is to calculate the Land Surface Emissivity (LSE) (ε) using Eq. (3):

$$\varepsilon = \varepsilon_v P_v + \varepsilon_s(1 - P_v) + C \quad (3)$$

with $\varepsilon_v = 0.986$, $\varepsilon_s = 0.97$, and $C = 0.004$.

3.1.2. Land Surface Temperature (LST)

a) Thermal Band to Brightness Temperature (TB)

The brightness temperature (TB) of the Earth's surface, which is a representation of the radiative temperature that the satellite sensor senses, was estimated using thermal infrared bands. Sensor-specific calibration constants included in each Landsat image's metadata were used to convert digital number (DN) values to spectral radiance and then to brightness temperature.

The following formula was first used to convert the thermal band (Band 6) for Landsat 5 TM (used for 2005) to Top-of-Atmosphere (TOA) spectral radiance (Lλ) Eq. 4.

$$L_\lambda = \left(\frac{L_{max} - L_{min}}{QCL_{max} - QCL_{min}}\right) \times (DN - QCAL_{min}) + L_{min} \quad (4)$$

where

L_{max} and L_{min} are the spectral radiance scaling factors, $QCAL_{MAX}$ and $QCAL_{MIN}$ represent the digital number (DN) range (typically 255 and 1 for 8-bit data), and L_λ is the spectral radiance in $W \cdot m^{-2} \cdot sr^{-1} \cdot \mu m^{-1}$.

The Brightness Temperature (TB) in Kelvin was then computed using the inverse of the Planck function by following Eq. 5.

$$T_B = \frac{K_2}{In\left(\frac{K_1}{L_\lambda} + 1\right)} \quad (5)$$

where

$K_1 = 607.76W \cdot m^{-2} \cdot sr^{-1} \cdot \mu m^{-1}$and $K_2 = 1260.56$K are the pre-launch calibration constants for Landsat 5 TM (Chander et al., 2009).

For Landsat 8 TIRS (used for 2015 and 2024), the thermal band (Band 10) was use, the radiance was computed using radiometric rescaling parameters that were taken straight from the metadata by Eq. 6.

$$L_\lambda = M_L \times Q_{cal} + A_L \quad (6)$$

where

$M_L$and $A_L$are the multiplicative and additive rescaling factors (RADIANCE_MULT_BAND_10 and RADIANCE_ADD_BAND_10) provided in the MTL metadata.

Brightness Temperature was derived similarly Eq. 7.

$$T_B = \frac{K_2}{In\left(\frac{K_1}{L_\lambda} + 1\right)} \quad (7)$$

using calibration constants $K_1 = 774.8853W \cdot m^{-2} \cdot sr^{-1} \cdot \mu m^{-1}$and $K_2 = 1321.0789$K (Barsi et al., 2003).

The satellite's measurement of the surface temperature before emissivity and atmospheric corrections is represented by the derived TB values. Following emissivity correction based on the vegetation fraction calculated from the NDVI, these values were used to estimate the Land Surface Temperature (LST).

b) Emissivity-Corrected LST: Eq. (7) can be used to calculate the LST based on the prior BT value that was determined by Eq. (8):

$$LST = \frac{T_B}{1 + (\lambda . {}^{T_B}/_{\rho}) . In(\varepsilon)} - 273.15 \quad (8)$$

where $\rho = 1.438 \times 10^{-2}$ m\cdotpK, $\lambda = 11.5 \times 10^{-6}$ m for Landsat 5/7, and $\lambda = 10.895 \times 10^{-6}$ m for Landsat 8 (J. A. Sobrino et al., 2004).

3.3.3. Vegetation Health Index (VHI)

The HVI integrates VCI and TCI to provide a combined indicator of vegetation health (Nanzad et al., 2019; Quiring & Ganesh, 2009). It is defined as Eq. 9

$$VHI = 0.5 \times VCI + 0.5 \times TCI \quad (9)$$

Where VCI is derived from NDVI (Kogan, 1995). It is expressed as Eq. 10

$$VCI = \frac{NDVI - NDVI_{min}}{NDVI_{max} - NDVI_{min}} \times 100 \quad (10)$$

Where TCI is derived from NDVI (Kogan, 1995). It is expressed as Eq. 11

$$TCI = \frac{LST_{max} - LST}{LST_{max} - LST_{min}} \times 100 \quad (11)$$

3.1.3. Urban heat island (UHI)

The Urban Heat Island (UHI) represents the relative temperature deviation of urban pixels compared to the citywide mean surface temperature. The UHI was quantified using a standardized normalization approach that expresses the deviation of each pixel's Land Surface Temperature (LST) from the mean LST of the entire study area (Schwarz et al., 2011; Xu et al., 2013). The UHI value calculation can be obtain by Eq. 12

$$UHI = \frac{LST - \overline{LST}}{\sigma_{LST}} \quad (12)$$

where LST is the land surface temperature (in Kelvin), $\overline{LST}$ is the mean LST of the study area, and σ_{LST} is the standard deviation of the LST.

3.1.4. Urban thermal field variance index (UTFVI)

The Urban Thermal Field Variance Index (UTFVI) was used to evaluate the degree of urban thermal stress and the ecological response to heat accumulation (H. Sun et al., 2009; J. A. Sobrino et al., 2012). UTFVI was computed using the following Eq. 13

$$UTFVI = \frac{LST - \overline{LST}}{\overline{LST}} \quad (13)$$

where LST is the temperature of each pixel and $\overline{LST}$ represents the mean LST across the image. The index classifies the urban surface into thermal stress categories ranging from "no thermal stress" to "strongest thermal stress", which were subsequently mapped to visualize heat accumulation zones and spatial thermal disparities across Rajshahi City.

4 Result and Discussion:

4.1 Spatiotemporal Dynamics of (NDVI) in 2005 to 2024

RCC's vegetation cover varies clearly over time and space, as seen in the NDVI maps for 2005, 2015, and 2024 Figure 3. While the Padma River and surrounding agricultural lands had higher NDVI values in 2005, the majority of built-up areas had low vegetation density, with NDVI values ranging from -0.59 to 0.16. As a result of roadside greening initiatives and afforestation, the NDVI significantly improved by 2015 (from -0.17 to 0.83), especially in the vicinity of Motihar and Rajshahi University area. Green cover remained in the northern and western peripheries in 2024, while the central and southern zones continued to lose vegetation as a result of urban densification, according to NDVI values (–0.34 to 0.82). The uneven spatial distribution of green spaces and the slow eradication of native vegetation in central Rajshahi due to continuous urban growth are generally highlighted by NDVI trends.

4.2 Spatiotemporal Dynamics of (VCI) in 2005 to 2024

The vegetation condition in Rajshahi City Corporation (RCC) exhibits significant temporal and spatial variations across the years 2005, 2015, and 2024 Figure 4. In 2005, vegetation health was relatively high across most parts of the city, with VCI values ranging from 10 to 88, indicating better vegetation moisture and productivity. By 2015, the overall Vegetation Condition Index

Figure 3. Spatiotemporal NDVI map from 2005, 2015 and 2024

(VCI) decreased (18–72), particularly in the central and southeastern regions, indicating heightened urban expansion and stress on vegetation. In contrast, 2024 shows partial recovery in several northern and western sectors, with VCI values between 25 and 84, likely due to localized green initiatives and vegetation regrowth. The southern built-up areas close to the Padma River still exhibit relatively poor vegetation conditions in spite of this improvement, indicating ongoing human pressure. The combined effects of land management techniques and urbanization on vegetation health in RCC over the previous 20 years are generally highlighted by the spatial pattern of VCI.

Figure 4. Spatiotemporal VCI map from 2005, 2015 and 2024

4.3 Variation of LST value over the year 2005, 2015 and 2024

The land surface temperature (LST) distribution in Rajshahi city for the years 2005, 2015, and 2024 is shown in (Fig. 5). The maps show clear patterns of surface temperature changes over time throughout the urban environment. With comparatively moderate thermal zones dispersed throughout the city, the LST in 2005 varied from 23.49°C to 38.57°C. The maximum LST rose to 42.36°C in 2015, indicating urbanization and a loss of vegetation cover, indicating a notable intensification of surface heating. The maximum temperature (41.34°C) on the 2024 map partially decreases, but elevated thermal zones still exist, especially in the city's center and north, which is indicative of continued urbanization and surface imperviousness. Cooler regions, mostly found close to the Padma River and surrounding green spaces, don't change much. Overall, the temporal sequence shows how RCC land-use changes and growing anthropogenic activities have gradually changed the city's thermal environment.

Figure 5. Spatiotemporal LST map from 2005, 2015 and 2024

4.5 Spatiotemporal Dynamics of (TCI) in 2005 to 2024

The Temperature Condition Index (TCI) for Rajshahi City Corporation (RCC) shows a clear change in space and time between 2005, 2015, and 2024 (Fig. 6). In 2005, TCI values ranged from 13 to 32. The northern and central areas had relatively good thermal conditions, but the southern zone along the Padma River showed moderate thermal stress. In 2015, TCI values dropped (17–27), which meant that the surface was heating up more and plants were under more stress, especially in the eastern and southern areas where cities were growing the most. The 2024 map shows that TCI has dropped even more (12–23), with low values being common in the central and western zones. Overall, the steady drop in TCI shows that urban heat is getting worse over time and surface moisture is getting lower, which is in line with RCC's loss of green cover and growth of impervious surfaces.

Figure 6. Spatiotemporal TCI map from 2005, 2015 and 2024

Figure 7. Spatiotemporal VHI map from 2005, 2015 and 2024

4.5 Spatiotemporal Dynamics of (VHI) in 2005 to 2024

The resilience and health of the vegetation in RCC are gradually declining, according to the VHI maps (fig. 7). The vegetation health in 2005 was moderate, with better conditions near the river

and agricultural zones, as indicated by VHI values ranging from 0.13 to 0.55. By 2015, VHI values had somewhat decreased (0.19–0.47) as the growing built-up land and rising temperatures put more stress on the central regions' vegetation. With a VHI ranging from 0.20 to 0.50 in 2024, the city's vegetation was under moderate to severe stress, especially in industrial belts and dense urban areas. Higher vegetation density typically translates into better vegetation health, and the spatial distribution of VHI closely matches that of NDVI. Nonetheless, the central and southern wards' consistently low VHI suggests that urban heat accumulation and scarce soil moisture have a growing impact on vegetation health.

4.6 Spatiotemporal Dynamics of UHI in 2005–2024

Figure 8. shows how the Urban Heat Island (UHI) intensity changed over time and space in RCC in 2005, 2015, and 2024. According to the analysis, the city's rapid urban expansion and the loss of vegetative cover are closely related to the noticeable and progressive intensification of surface thermal conditions over the past 20 years. The central wards and the northern built-up zones were the main locations for moderate thermal hotspots in 2005, when UHI values varied from –2.67°C to 2.41°C. Due to the combined effects of open green spaces, riverine moisture, and low construction density, a significant portion of the city remained cooler at that time, especially along the southern and southwestern edges close to the Padma River. Given RCC early urbanization, the thermal environment was comparatively balanced. With values ranging from –6.22°C to 4.73°C, UHI intensity had significantly increased by 2015. The urban core saw a significant expansion of thermal hotspots, particularly in the Motihar, Boalia, and Rajpara areas, where impervious materials predominated and rapid infrastructure development was common. The overall pattern showed a distinct shift toward widespread thermal stress, even though the southern and southeastern portions of the city, including the areas near rivers, continued to have cooler microclimates. RCC’s rapid urbanization and increasing population density during this time frame are known to increase anthropogenic heat release and decrease evapotranspiration. With a high of 4.97°C and a low of –3.79°C in 2024, the UHI pattern peaked in intensity. Particularly over the northern and central sectors, where urban land cover currently predominates, hotspots grew in size and intensity.

Figure 8. Spatiotemporal UHI map from 2005, 2015 and 2024

Figure 8. Spatiotemporal VHI map from 2005, 2015 and 2024

4.7 Spatiotemporal Dynamics of UTFVI in 2005–2024

The UTFVI maps show a spatial pattern that closely resembles the distribution of UHI. Low to moderate ecological stress was indicated by UTFVI values in 2005, which varied from -0.33 to 0.18. The range increased to -0.53 to 0.20 by 2015, suggesting that the same urban cores where UHI hotspots were detected had seen an increase in thermal stress and related ecological degradation. Even greater levels of stress are depicted on the 2024 UTFVI map (range: –0.30 to 0.23), particularly in the city's central and northern regions. A clear link between rising surface temperatures and declining urban ecological quality is confirmed by the high UTFVI values that correlate to regions of elevated UHI.

Figure 9. Spatiotemporal UTFVI map from 2005, 2015 and 2024

4.8. Ward-Wise Changes in Land Surface Temperature, UHI, and UTFVI

The mean Land Surface Temperature (LST), Urban Heat Island (UHI) intensity, and Urban Thermal Field Variance Index (UTFVI) for each of Rajshahi City Corporation's thirty wards between 2005 and 2024 are compared ward-by-ward in Figure 10. The findings show that during the course of the study, surface temperature and urban heat stress clearly increased.

According to the LST profile, most wards' mean surface temperatures in 2024 are continuously higher than those in 2005. The highest LST values are seen in the central and western wards, especially Wards 5–13, which indicate increased surface heating. Rapid urban growth, an increase in impermeable surfaces, and a decrease in plant cover are the main causes of this surge. Peripheral wards, on the other hand, exhibit comparatively lower LST levels, indicating more greenery and less urban growth.

The urban heat effects' gradual development is further highlighted by the UHI research. The majority of wards showed low or slightly positive UHI readings in 2005, suggesting that there was little temperature differential between urban and outlying areas. But by 2024, UHI intensity has significantly increased, particularly in the western and central wards (Wards 5–13), where values often surpass 1.0, indicating a strong urban heat island creation. The UHI values in the peripheral wards (Wards 25–29) are lower or even negative, indicating relatively cooler surface conditions linked to more green coverage and lower built-up density.

In a similar way, the UTFVI results show that urban thermal stress increased significantly between 2005 and 2024. The majority of wards had low or negative UTFVI readings in 2005, indicating a rather balanced urban thermal climate. By 2024, a number of western and central wards exhibit positive UTFVI readings, signifying worsening thermal comfort conditions and greater ecological stress. The periphery wards, on the other hand, continue to have low or negative UTFVI readings, which are indicative of less urbanization pressure and better weather. Overall, Figure 10 clearly shows the spatiotemporal expansion of urban heat stress in Rajshahi City, with the outside wards remaining more thermally stable while central and western wards developing as critical hotspots as a result of increased urbanization and deforestation.

Figure 10. Ward-wise variation of mean Land Surface Temperature (LST), Urban Heat Island (UHI), and Urban Thermal Field Variance Index (UTFVI) in Rajshahi City Corporation (RCC) for 2005 and 2024.

5. Correlation

Fig. 11. utilizes scatter plots with fitted linear trend lines to show the pairwise correlations between important environmental indices for RCC, including NDVI, LST, VCI, TCI, VHI, and UHI. Because of the cooling effect of urban and peri-urban vegetation, areas with higher vegetation cover typically experience lower land surface temperatures, according to the NDVI–

Figure 11. Vegetation, thermal, drought, and urban heat index correlations in RCC

LST relationship, which clearly shows a negative correlation. The UHI–NDVI plot also shows a negative correlation, indicating that more vegetation lowers the intensity of urban heat islands. The VCI–TCI plot shows a negative correlation, indicating that as thermal stress rises, vegetation stress also rises. The Vegetation Health Index (VHI) is mutually influenced by vegetation condition (VCI) and thermal condition (TCI), with improving vegetation and thermal conditions leading to greater overall vegetation health, as demonstrated by the positive correlations between VCI–VHI and TCI–VHI. Lastly, the VHI–UHI connection shows a very modest positive trend, suggesting that changes in urban heat intensity very slightly affect vegetation health. This is probably because of the combined effects of thermal stress and vegetation cover in diverse urban contexts.

5. Conclusion:

- This study investigated the spatiotemporal dynamics of urban heat conditions and vegetation health in Rajshahi City Corporation from 2005 to 2024, using multi-temporal

Landsat images and the Google Earth Engine platform. The study offers a thorough evaluation of how fast urbanization has affected the city's thermal and ecological environment by integrating Land Surface Temperature (LST), NDVI, VCI, TCI, VHI, Urban Heat Island (UHI), and Urban Thermal Field Variance Index (UTFVI) at the ward level.

- The findings show that during the previous 20 years, surface temperature and urban heat stress have clearly increased, with central and western wards emerging as enduring thermal hotspots. Higher LST, stronger UHI intensity, and higher UTFVI values were found in areas with impermeable surfaces and high built-up density, whereas vegetated and river-adjacent zones consistently displayed lower thermal stress. The urban core's deteriorating trends in NDVI, VCI, TCI, and VHI attest to rising ecological stress and vegetation degradation brought on by an increase in urban land cover.
- The crucial function that urban greenery plays in reducing heat accumulation is further shown by ward-wise and correlation analyses that show a strong inverse link between vegetation indices and thermal indicators. In order to enhance thermal comfort and ecological resilience, the results highlight the significance of incorporating vegetation conservation and nature-based solutions into urban development.

Funding

No Funding is available.

Declaration of competing interest

The authors declare that they have no known competing financial interests or personal relationships that could have appeared to influence the work reported in this paper.

6. References

Al Rakib, A., Akter, K. S., Rahman, M. N., Arpi, S., & Kafy, A.-A. (2020, December 6). Analyzing the pattern of land use land cover change and its impact on land surface temperature: A remote sensing approach in Mymensingh, Bangladesh. In Proceedings of the 1st International Student Research Conference 2020, Dhaka University Research Society, Dhaka, Bangladesh.

Bala, R., Prasad, R., & Yadav, V. P. (2021). Quantification of Urban Heat Intensity with Land Use/Land Cover Changes Using Landsat Satellite Data Over Urban Landscapes. *Research Square (Research Square)*. https://doi.org/10.21203/rs.3.rs-243576/v1

Barsi, J. A., Barker, J. L., & Schott, J. R. (2003). An atmospheric correction parameter calculator for a single thermal band earth-sensing instrument. In Proceedings of the IEEE International Geoscience and Remote Sensing Symposium (IGARSS), Vol. 5, pp. 3014–3016.

Cetin, Z., & Yastikli, N. (2022). The use of machine learning algorithms in urban tree species classification. ISPRS International Journal of Geo-Information, 11(4), 226. https://doi.org/10.3390/ijgi11040226

Chakraborty, T., & Lee, X. (2018). A simplified urban-extent algorithm to characterize surface urban heat islands on a global scale and examine vegetation control on their spatiotemporal variability. International Journal of Applied Earth Observation and Geoinformation, 74, 269–280. https://doi.org/10.1016/j.jag.2018.09.015

Chander, G., Markham, B. L., & Helder, D. L. (2009). Summary of current radiometric calibration coefficients for Landsat MSS, TM, ETM+, and EO-1 ALI sensors. Remote Sensing of Environment, 113(5), 893–903. https://doi.org/10.1016/j.rse.2009.01.007

Clemett, A., Amin, M. M., Ara, S., & Akan, M. M. R. (2006). *Background information for Rajshahi City, Bangladesh* (Unpublished report). Bangladesh Institute of Planners.

Dey, N. N., Rakib, A. A., Kafy, A.-. A., & Raikwar, V. (2021). Geospatial modelling of changes in land use/land cover dynamics using Multi-layer Perceptron Markov chain model in Rajshahi City, Bangladesh. *Environmental Challenges*, *4*, 100148. https://doi.org/10.1016/j.envc.2021.100148

Ferdous, M., & Baten, M. (2012). Climatic Variables of 50 Years and their Trends over Rajshahi and Rangpur Division. *Journal of Environmental Science and Natural Resources*, *4*(2), 147–150. https://doi.org/10.3329/jesnr.v4i2.10165

Ghobadi, Y., Pradhan, B., Shafri, H. Z. M., & Kabiri, K. (2013). Assessment of spatial relationship between land surface temperature and landuse/cover retrieval from multi-temporal remote sensing data in South Karkheh Sub-basin, Iran. Arabian Journal of Geosciences, 8(1), 525–537. https://doi.org/10.1007/s12517-013-1244-3

Gorelick, N., Hancher, M., Dixon, M., Ilyushchenko, S., Thau, D., & Moore, R. (2017). Google Earth Engine: Planetary-scale geospatial analysis for everyone. *Remote Sensing of Environment*, *202*, 18–27. https://doi.org/10.1016/j.rse.2017.06.031

Grimmond, S. (2007). Urbanization and global environmental change: local effects of urban warming. *Geographical Journal*, *173*(1), 83–88. https://doi.org/10.1111/j.1475-4959.2007.232_3.x

Guha, S., Govil, H., Dey, A., & Gill, N. (2018). Analytical study of land surface temperature with NDVI and NDBI using Landsat 8 OLI and TIRS data in Florence and Naples city, Italy. *European Journal of Remote Sensing*, *51*(1), 667–678. https://doi.org/10.1080/22797254.2018.1474494

Guo, G., Wu, Z., Xiao, R., Chen, Y., Liu, X., & Zhang, X. (2014). Impacts of urban biophysical composition on land surface temperature in urban heat island clusters. *Landscape and Urban Planning*, *135*, 1–10. https://doi.org/10.1016/j.landurbplan.2014.11.007

Imhoff, M. L., Zhang, P., Wolfe, R. E., & Bounoua, L. (2009). Remote sensing of the urban heat island effect across biomes in the continental USA. *Remote Sensing of Environment*, *114*(3), 504–513. https://doi.org/10.1016/j.rse.2009.10.008

Kafy, A. A., Al-Faisal, A., Hasan, M. M., Sikdar, S., Khan, M. H. H., Rahman, M., & Islam, R. (2019). Impact of LULC changes on LST in Rajshahi District of Bangladesh: A remote sensing approach. Journal of Geographical Studies, 3(1), 11–23.

Kafy, A.-. A., Abdullah-Al-Faisal, N., Rahman, M. S., Islam, M., Rakib, A. A., Islam, M. A., Khan, M. H. H., Sikdar, M. S., Sarker, M. H. S., Mawa, J., & Sattar, G. S. (2020). Prediction of seasonal urban thermal field variance index using machine learning algorithms in Cumilla, Bangladesh. *Sustainable Cities and Society*, *64*, 102542. https://doi.org/10.1016/j.scs.2020.102542

Karnieli, A., Agam, N., Pinker, R. T., Anderson, M., Imhoff, M. L., Gutman, G. G., Panov, N., & Goldberg, A. (2009). Use of NDVI and land surface temperature for drought assessment: Merits and limitations. *Journal of Climate*, *23*(3), 618–633. https://doi.org/10.1175/2009jcli2900.1

Kavlak, M. O., Cabuk, S. N., & Cetin, M. (2021). Development of forest fire risk map using geographical information systems and remote sensing capabilities: Ören case. *Environmental Science and Pollution Research*, *28*(25), 33265–33291. https://doi.org/10.1007/s11356-021-13080-9

Khaliq, A., Musci, M. A., & Chiaberge, M. (2018). *Analyzing relationship between maize height and spectral indices derived from remotely sensed multispectral imagery.* In *Proceedings of the 2018 IEEE Applied Imagery Pattern Recognition Workshop (AIPR 2018)* (pp. 1–5). IEEE. https://doi.org/10.1109/AIPR.2018.8707373

Kogan, F. (1995). Application of vegetation index and brightness temperature for drought detection. Advances in Space Research, 15(11), 91–100. https://doi.org/10.1016/0273-1177(95)00079-t

Li, C., Zhao, J., Thinh, N. X., Yang, W., & Li, Z. (2018). Analysis of the spatiotemporally varying effects of urban spatial patterns on land surface temperatures. *Journal of Environmental Engineering and Landscape Management, 26*(3), 216–231. https://doi.org/10.3846/jeelm.2018.5378

Liu, W. T., & Kogan, F. (2002). Monitoring Brazilian soybean production using NOAA/AVHRR based vegetation condition indices. *International Journal of Remote Sensing*, *23*(6), 1161–1179. https://doi.org/10.1080/01431160110076126

Marufuzzaman, M., Khanam, M. M., & Hasan, M. K. (2021). Monitoring the Land Cover Change and Its Impact on the Land Surface Temperature of Rajshahi City, Bangladesh using GIS and Remote Sensing Techniques. *Journal of Geography Environment and Earth Science International*, 1–19. https://doi.org/10.9734/jgeesi/2021/v25i430278

Nanzad, L., Zhang, J., Tuvdendorj, B., Nabil, M., Zhang, S., & Bai, Y. (2019). NDVI anomaly for drought monitoring and its correlation with climate factors over Mongolia from 2000 to 2016. *Journal of Arid Environments*, *164*, 69–77. https://doi.org/10.1016/j.jaridenv.2019.01.019

Oke, T. R. (1982). The energetic basis of the urban heat island. *Quarterly Journal of the Royal Meteorological Society*, *108*(455), 1–24. https://doi.org/10.1002/qj.49710845502

Quiring, S. M., & Ganesh, S. (2009). Evaluating the utility of the Vegetation Condition Index (VCI) for monitoring meteorological drought in Texas. *Agricultural and Forest Meteorology*, *150*(3), 330–339. https://doi.org/10.1016/j.agrformet.2009.11.015

Rahman, M. M., & Hasan, J. (2024). Evaluating the impact of green spaces on urban heat reduction in Rajshahi, Bangladesh using the INVEST model. Land, 13(8), 1284. https://doi.org/10.3390/land13081284

Rahman, M. N., Rony, M. R. H., Jannat, F. A., Pal, S. C., Islam, M. S., Alam, E., & Islam, A. R. M. T. (2022). Impact of urbanization on urban heat island intensity in major districts of Bangladesh using remote sensing and Geo-Spatial tools. *Climate*, *10*(1), 3. https://doi.org/10.3390/cli10010003

Rahman, M. R., & Mark, B. G. (2025). Geospatial Analysis of Urban Warming: A remote sensing and GIS-Based investigation of winter land surface temperature and biophysical

composition in Rajshahi City, Bangladesh. Sustainability, 17(11), 5107. https://doi.org/10.3390/su17115107

Rajdhani Development Authority. (2003, 2008). *Dhaka metropolitan master plan 2003–2015; Dhaka detailed area plan 2008*. Rajdhani Development Authority, Government of Bangladesh.

Rizwan, A. M., Dennis, L. Y., & Liu, C. (2008). A review on the generation, determination and mitigation of Urban Heat Island. *Journal of Environmental Sciences*, *20*(1), 120–128. https://doi.org/10.1016/s1001-0742(08)60019-4

Roy, S., Biswas, A., Shawon, M. T. A., Akter, S., & Rahman, M. M. (2024). Land use and meteorological influences on dengue transmission dynamics in Dhaka city, Bangladesh. *Bulletin of the National Research Centre/Bulletin of the National Research Center*, *48*(1). https://doi.org/10.1186/s42269-024-01188-0

Sadat, N., Sheikh, H., & Asaduzzaman, M. (2024). Evaluating urban heat island mitigation strategies in Rajshahi, using ENVI-MET: a remote sensing approach. Journal of Contemporary Urban Affairs, 8(2). https://doi.org/10.25034/ijcua.2024.v8n2-15

Santamouris, M. (2015). Analyzing the heat island magnitude and characteristics in one hundred Asian and Australian cities and regions. *The Science of the Total Environment*, *512–513*, 582–598. https://doi.org/10.1016/j.scitotenv.2015.01.060

Schwarz, N., Lautenbach, S., & Seppelt, R. (2011). Exploring indicators for quantifying surface urban heat islands of European cities with MODIS land surface temperatures. *Remote Sensing of Environment*, *115*(12), 3175–3186. https://doi.org/10.1016/j.rse.2011.07.003

Sobrino, J. A., Jiménez-Muñoz, J. C., & Paolini, L. (2004). Land surface temperature retrieval from LANDSAT TM 5. *Remote Sensing of Environment*, *90*(4), 434–440. https://doi.org/10.1016/j.rse.2004.02.003

Sobrino, J. A., Oltra-Carrió, R., Sòria, G., Jiménez-Muñoz, J. C., Franch, B., Hidalgo, V., Mattar, C., Julien, Y., Cuenca, J., Romaguera, M., Gómez, J. A., De Miguel, E., Bianchi, R., & Paganini, M. (2012). Evaluation of the surface urban heat island effect in the city of Madrid by thermal remote sensing. *International Journal of Remote Sensing*, *34*(9–10), 3177–3192. https://doi.org/10.1080/01431161.2012.716548

Sobrino, J., García-Monteiro, S., & Julien, Y. (2020). Surface Temperature of the Planet Earth from Satellite Data over the Period 2003–2019. *Remote Sensing*, *12*(12), 2036. https://doi.org/10.3390/rs12122036

562 Sun, B., Calbet, X., Reale, A., Schroeder, S., Bali, M., Smith, R., & Pettey, M. (2021). Accuracy
563 of Vaisala RS41 and RS92 upper tropospheric humidity compared to satellite hyperspectral
564 infrared measurements. *Remote Sensing*, *13*(2), 173. https://doi.org/10.3390/rs13020173

565 Sun, H., Huang, J., Huete, A. R., Peng, D., & Zhang, F. (2009). Mapping paddy rice with multi-
566 date moderate-resolution imaging spectroradiometer (MODIS) data in China. *Journal of*
567 *Zhejiang University. Science A*, *10*(10), 1509–1522. https://doi.org/10.1631/jzus.a0820536

568 **USGS (2024).** *Landsat 8 (L8) Data Users Handbook.* U.S. Geological Survey, Earth Resources
569 Observation and Science (EROS) Center. Available at: https://landsat.usgs.gov

570 Voogt, J., & Oke, T. (2003). Thermal remote sensing of urban climates. *Remote Sensing of*
571 *Environment*, *86*(3), 370–384. https://doi.org/10.1016/s0034-4257(03)00079-8

572 Weng, Q. (2009). Thermal infrared remote sensing for urban climate and environmental studies:
573 Methods, applications, and trends. *ISPRS Journal of Photogrammetry and Remote Sensing*,
574 *64*(4), 335–344. https://doi.org/10.1016/j.isprsjprs.2009.03.007

575 Xu, D., Guo, X., Li, Z., Yang, X., & Yin, H. (2013). Measuring the dead component of mixed
576 grassland with Landsat imagery. *Remote Sensing of Environment*, *142*, 33–43.
577 https://doi.org/10.1016/j.rse.2013.11.017

578 Yang, Y., Anderson, M., Gao, F., Xue, J., Knipper, K., & Hain, C. (2022). Improved daily
579 evapotranspiration estimation using remotely sensed data in a data fusion system. *Remote*
580 *Sensing*, *14*(8), 1772. https://doi.org/10.3390/rs14081772

581 Yang, Y., Cai, W., & Yang, J. (2017). Evaluation of MODIS land Surface temperature data to
582 estimate Near-Surface Air temperature in Northeast China. *Remote Sensing*, *9*(5), 410.
583 https://doi.org/10.3390/rs9050410

584 Zhou, D., Zhao, S., Liu, S., Zhang, L., & Zhu, C. (2014). Surface urban heat island in China's 32 major
585 cities: Spatial patterns and drivers. *Remote Sensing of Environment*, *152*, 51–61.
586 https://doi.org/10.1016/j.rse.2014.05.017

587

588

589

590

591

592

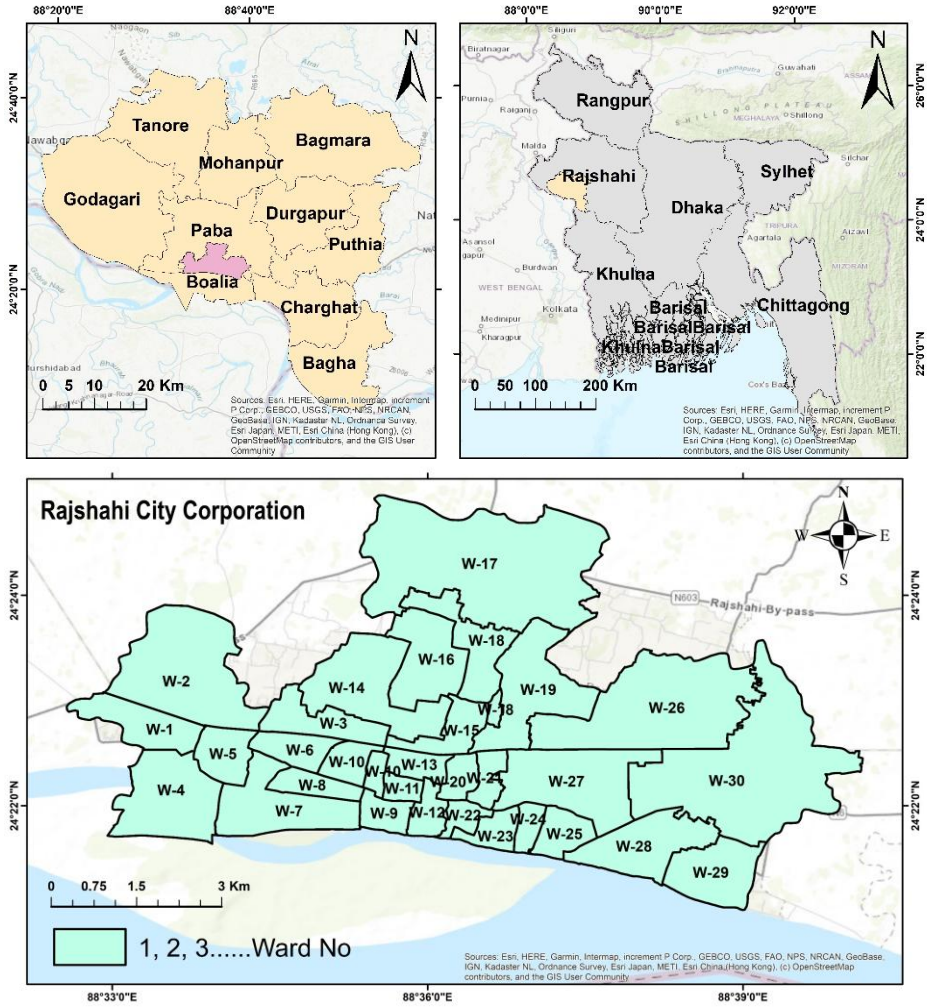


Figure 1. Study area map

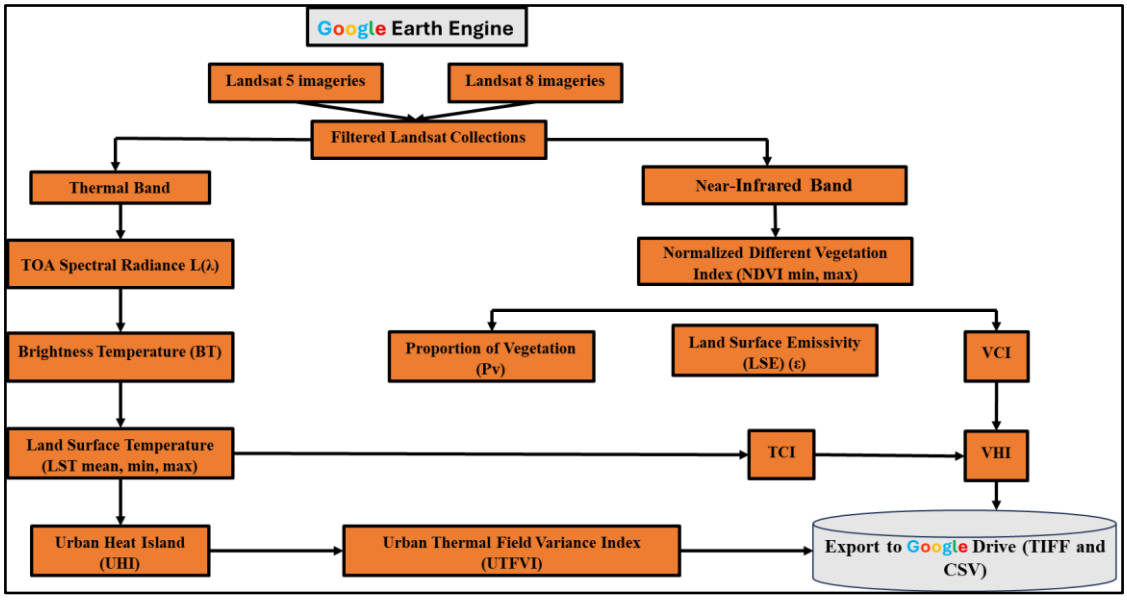


Figure 2. Flowchart of data processing.

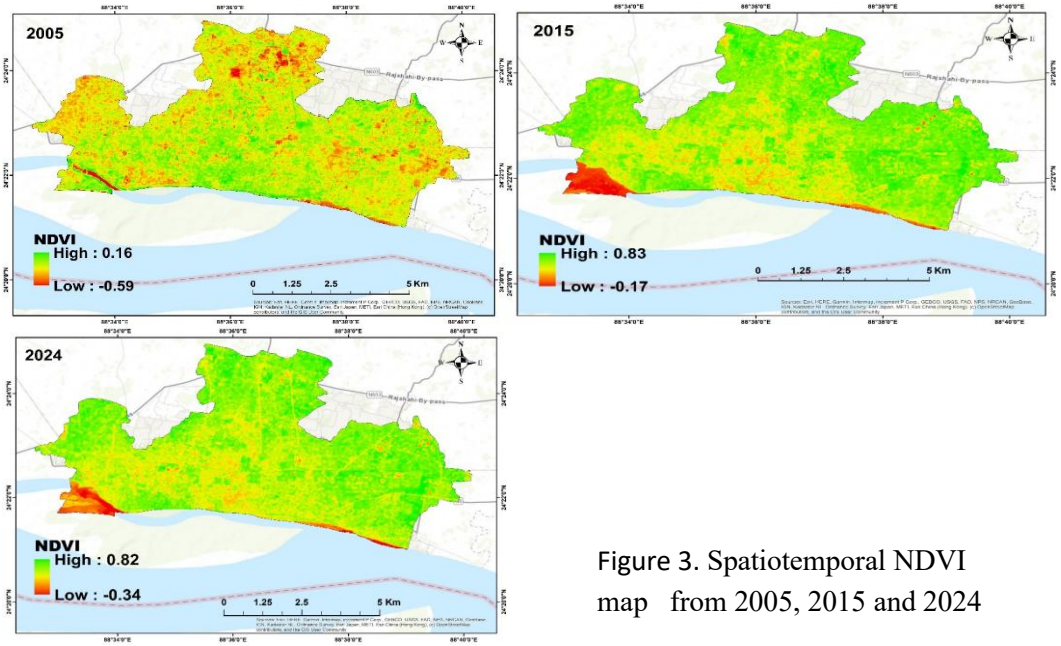


Figure 3. Spatiotemporal NDVI map from 2005, 2015 and 2024

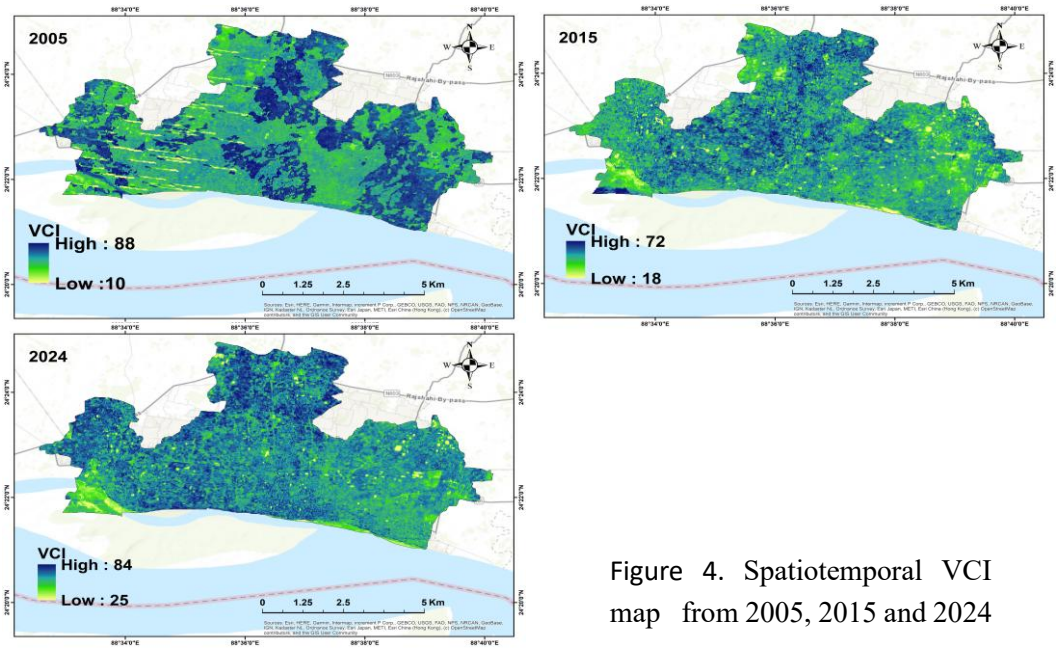


Figure 4. Spatiotemporal VCI map from 2005, 2015 and 2024

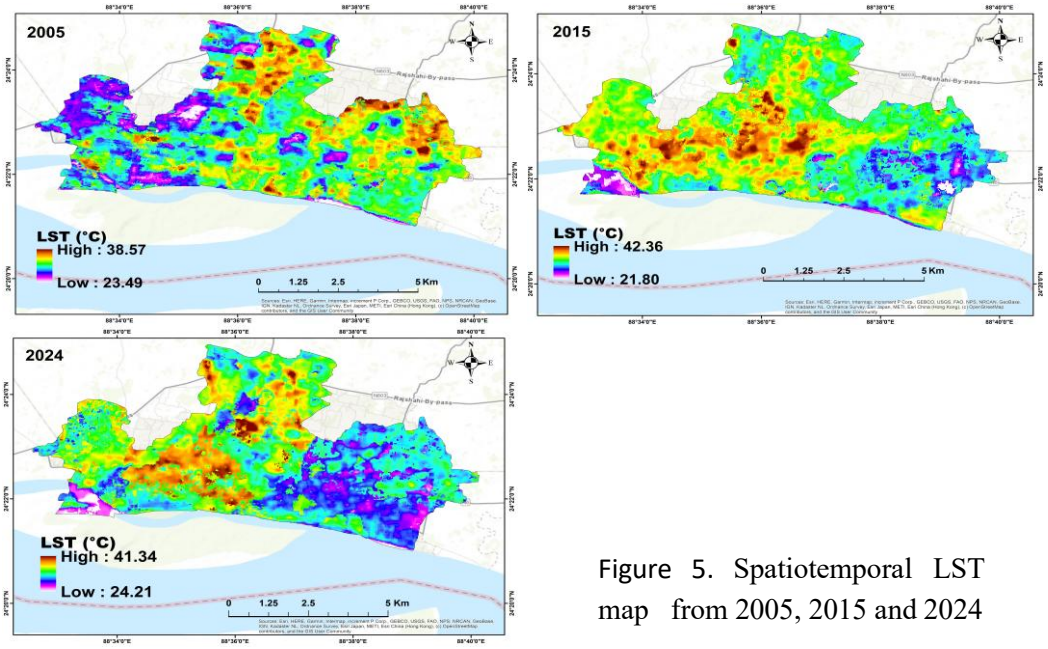


Figure 5. Spatiotemporal LST map from 2005, 2015 and 2024

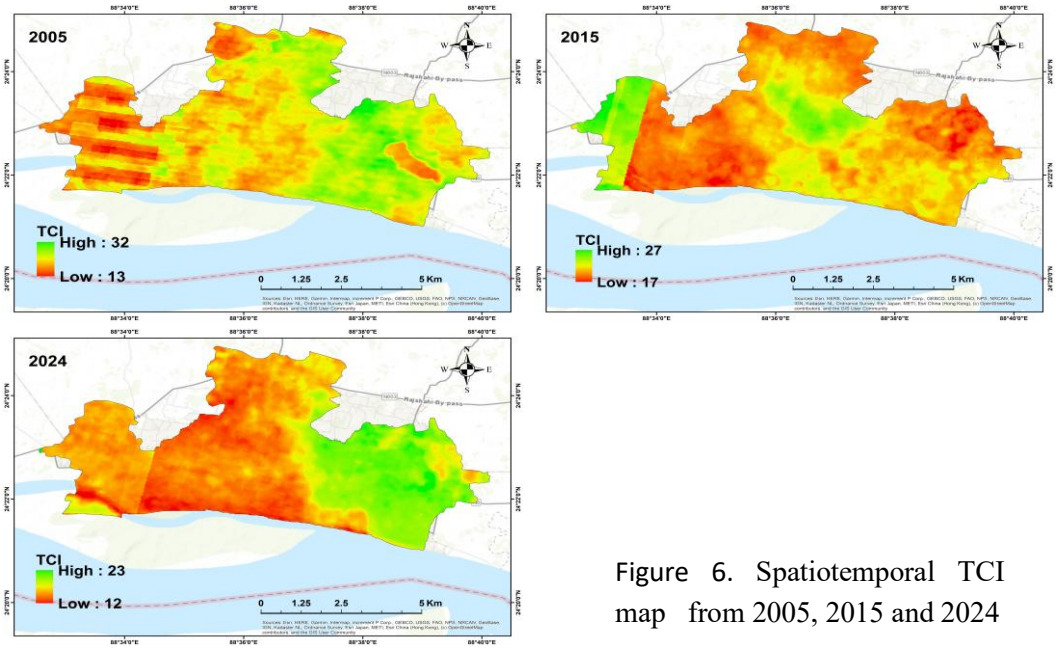


Figure 6. Spatiotemporal TCI map from 2005, 2015 and 2024

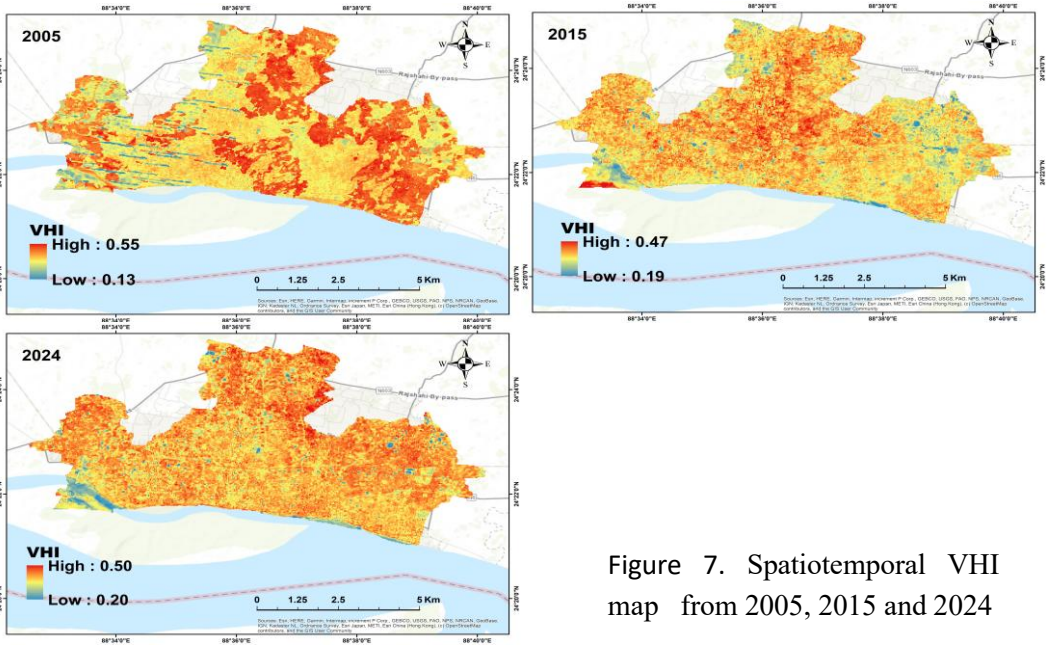


Figure 7. Spatiotemporal VHI map from 2005, 2015 and 2024

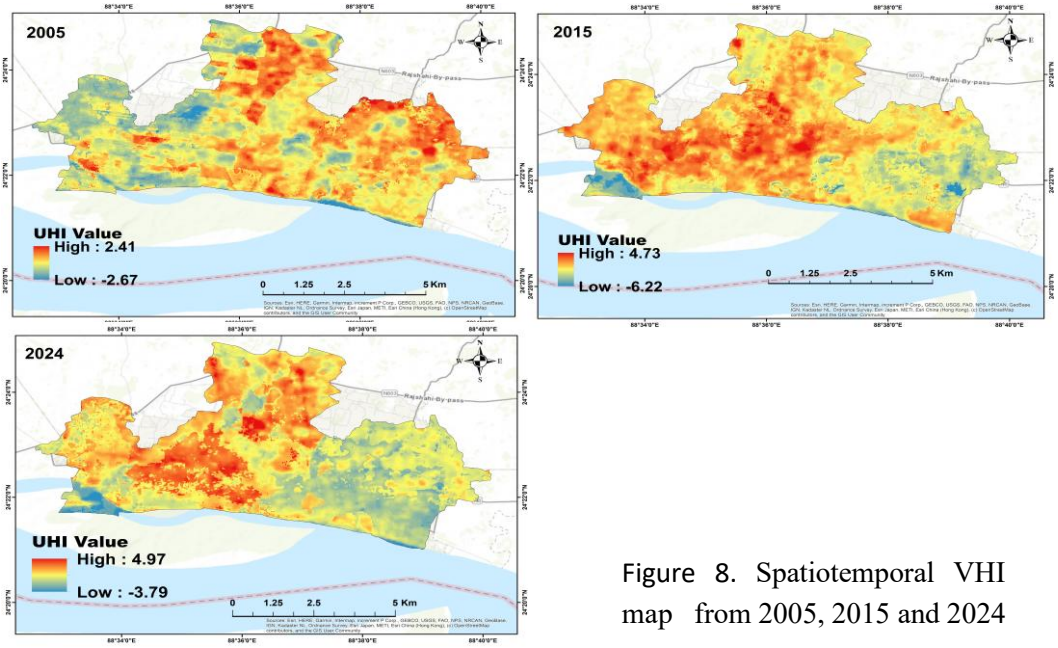


Figure 8. Spatiotemporal VHI map from 2005, 2015 and 2024

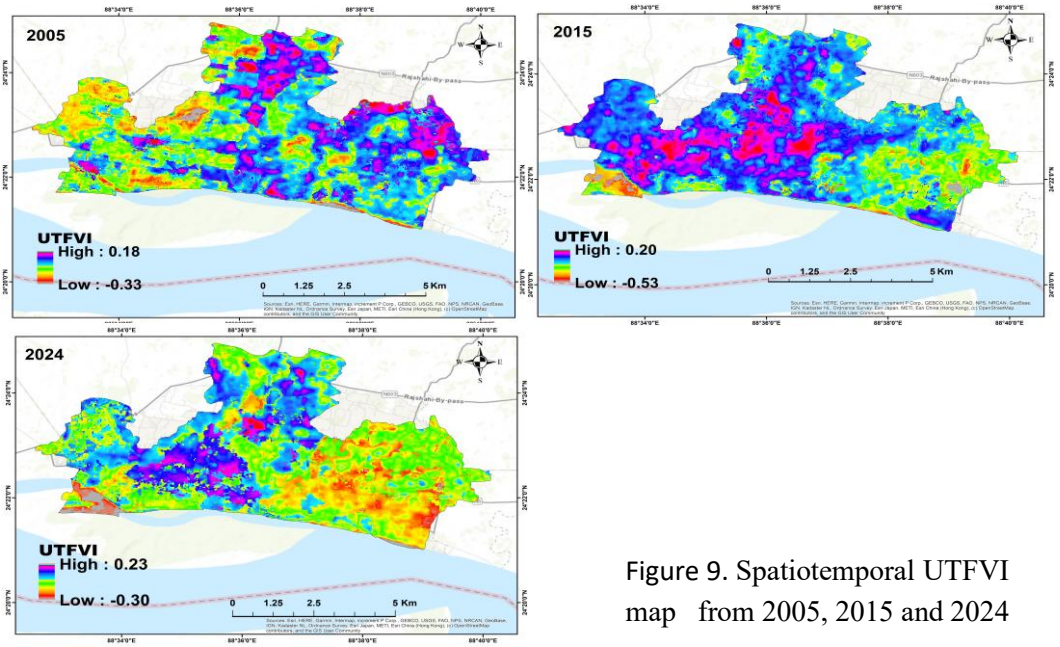


Figure 9. Spatiotemporal UTFVI map from 2005, 2015 and 2024

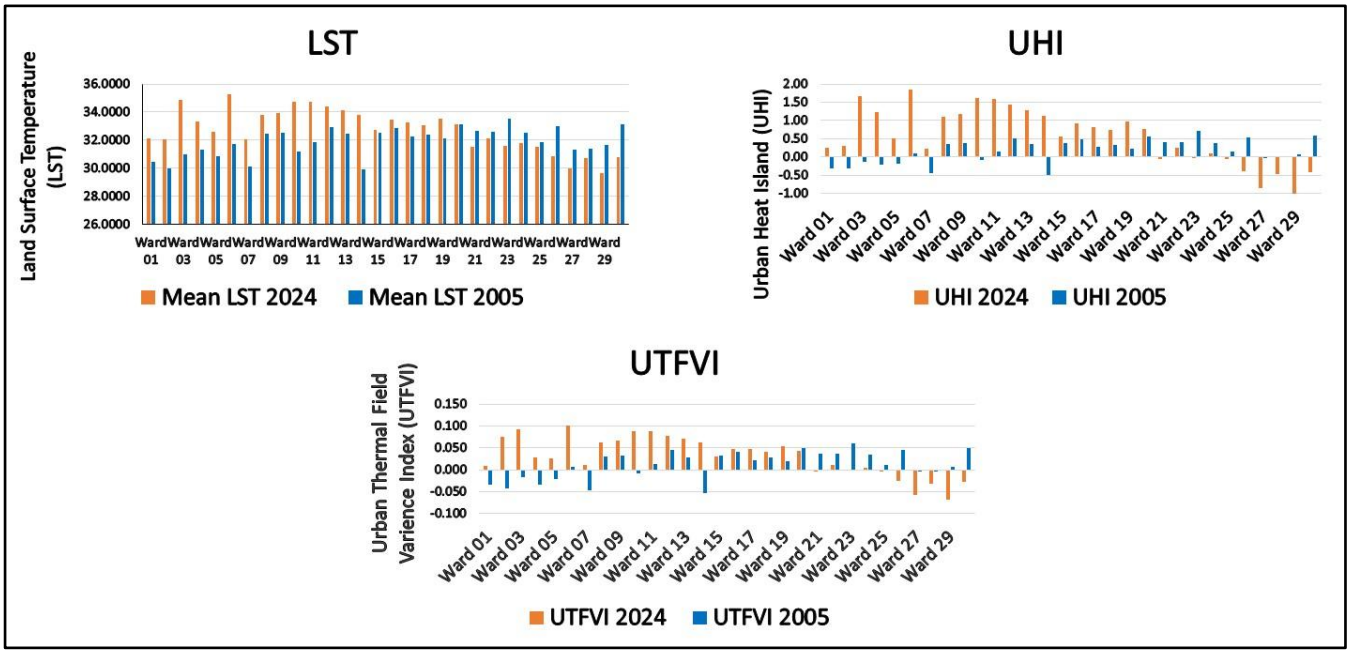


Figure 10. Ward-wise variation of mean Land Surface Temperature (LST), Urban Heat Island (UHI), and Urban Thermal Field Variance Index (UTFVI) in Rajshahi City Corporation (RCC) for 2005 and 2024.

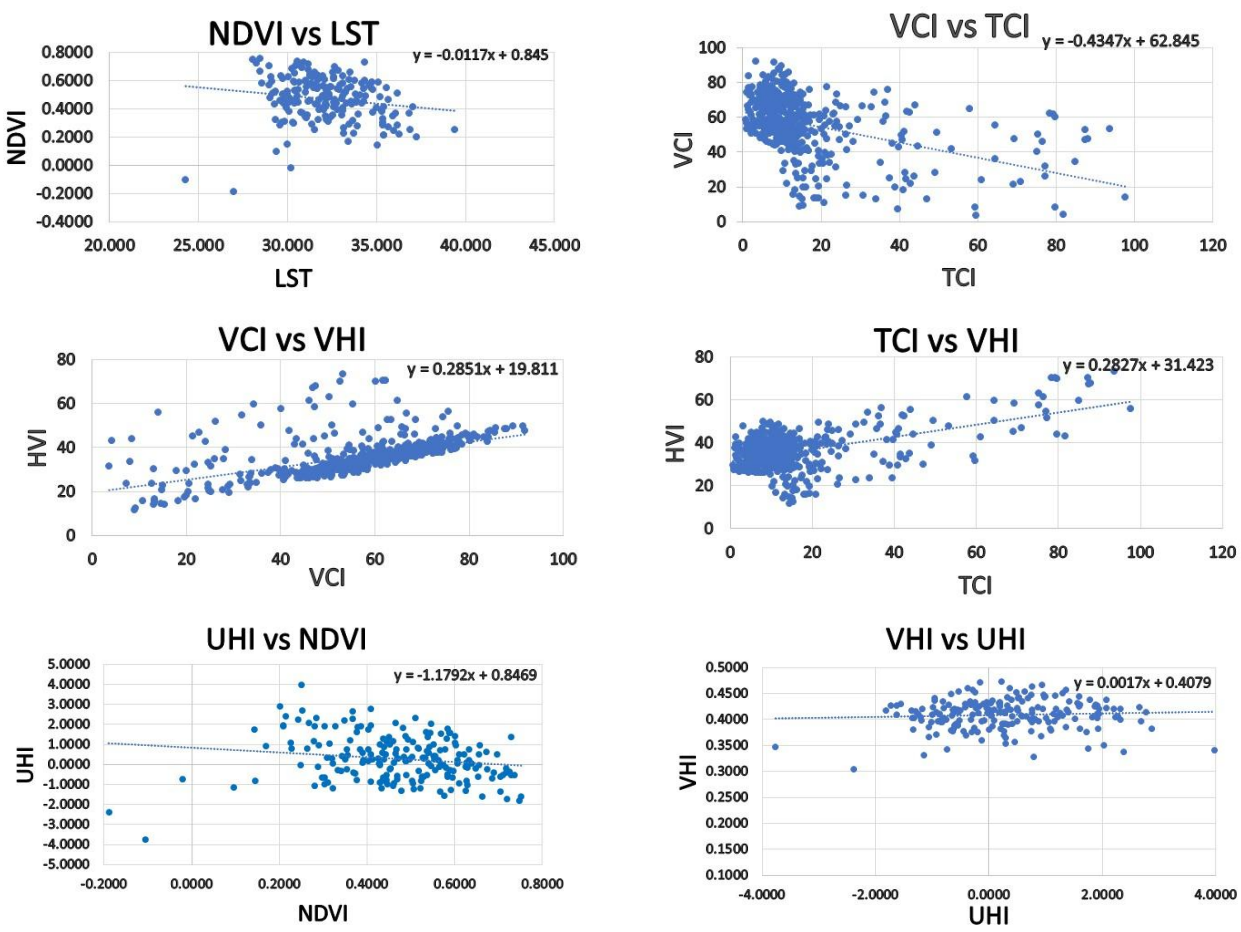


Figure 11. Vegetation, thermal, drought, and urban heat index correlations in RCC